

Measurement of ^1H - ^{15}N and ^1H - ^{13}C residual dipolar couplings in nucleic acids from TROSY intensities

Jinfa Ying · Jinbu Wang · Alex Grishaev ·
Ping Yu · Yun-Xing Wang · Ad Bax

Received: 5 May 2011 / Accepted: 22 June 2011
© Springer Science+Business Media B.V. (outside the USA) 2011

Abstract Analogous to the recently introduced ARTSY method for measurement of one-bond ^1H - ^{15}N residual dipolar couplings (RDCs) in large perdeuterated proteins, we introduce methods for measurement of base ^{13}C - ^1H and ^{15}N - ^1H RDCs in protonated nucleic acids. Measurements are based on quantitative analysis of intensities in ^1H - ^{15}N and ^{13}C - ^1H TROSY-HSQC spectra, and are illustrated for a 71-nucleotide adenine riboswitch. Results compare favorably with those of conventional frequency-based measurements in terms of completeness and convenience of use. The ARTSY method derives the size of the coupling from the ratio of intensities observed in two TROSY-HSQC spectra recorded with different dephasing delays, thereby minimizing potential resonance overlap problems. Precision of the RDC measurements is limited by the signal-to-noise ratio, S/N, achievable in the 2D TROSY-HSQC reference spectrum, and is approximately given by $30/(S/N)$ Hz for ^{15}N - ^1H and $65/(S/N)$ Hz for ^{13}C - ^1H . The signal-to-noise ratio of both ^1H - ^{15}N and ^1H - ^{13}C spectra greatly benefits when water magnetization during the

experiments is not perturbed, such that rapid magnetization transfer from bulk water to the nucleic acid, mediated by rapid amino and hydroxyl hydrogen exchange coupled with ^1H - ^1H NOE transfer, allows for fast repetition of the experiment. RDCs in the mutated helix 1 of the riboswitch are compatible with nucleotide-specific modeled, idealized A-form geometry and a static orientation relative to the helix 2/3 pair, which differs by ca 6° relative to the X-ray structure of the native riboswitch.

Keywords ARTSY · BEST · A-form RNA · Quantitative J correlation · TROSY · RDC · RNA · DNA

Introduction

It is well recognized that residual dipolar couplings, as measured by solution state NMR, carry important structural information regarding internuclear vector orientation relative to the principal axis system of the molecule's alignment tensor. This "global" information complements local structural restraints derived from NOE, chemical shift, and J-coupling measurements and has proven useful in biomolecular structure determination (Clare 2000; Prestegard et al. 2000; Bax and Grishaev 2005; Tolman and Ruan 2006). Moreover, RDCs can provide important information on dynamic processes that can remain elusive by conventional relaxation measurements, both in proteins (Peti et al. 2002; Tolman 2002; Bouvignies et al. 2005; Yao et al. 2008) and in nucleic acids (Zhang et al. 2006, 2007). A wide range of different types of RDCs has been measured, including ^1H - ^{15}N , ^1H - ^{13}C , ^1H - ^1H , ^{15}N - ^{13}C , and ^{13}C - ^{13}C (Tjandra and Bax 1997a, b; Yang et al. 1999; Permi et al. 2000; Skrynnikov et al. 2000; Skrynnikov and Kay 2000; Evenas et al. 2001; Boisbouvier et al. 2003; Vijayan and

This manuscript is dedicated to Professor Lewis E. Kay, on the occasion of his 50th birthday.

Electronic supplementary material The online version of this article (doi:10.1007/s10858-011-9544-y) contains supplementary material, which is available to authorized users.

J. Ying · A. Grishaev · A. Bax (✉)
Laboratory of Chemical Physics, National Institute of Diabetes and Digestive and Kidney Diseases, National Institutes of Health, Building 5, Room 126, Bethesda, MD 20892-0520, USA
e-mail: bax@nih.gov

J. Wang · P. Yu · Y.-X. Wang
Structural Biophysics Laboratory, National Cancer Institute, National Institutes of Health, Frederick, MD 21702, USA

Zweckstetter 2005), and many of these interactions can be measured even in lowly populated transient conformers, not directly visible by conventional NMR (Hansen et al. 2008a, b; Vallurupalli et al. 2008; van Ingen et al. 2009). However, in larger slowly tumbling systems, measurements are often restricted to the backbone amide ^1H - ^{15}N RDC for proteins, and the imino ^1H - ^{15}N RDC for base-paired nucleic acids.

A recently introduced method, ARTSY, yields ^1H - ^{15}N amide RDCs in perdeuterated proteins from analysis of the intensity ratio in two TROSY-HSQC spectra, recorded with different dephasing delays (Fitzkee and Bax 2010), and provides facile measurement of $^1\text{D}_{\text{NH}}$ RDCs in larger proteins. Here, we present methods based on the ARTSY concept for measuring ^1H - ^{15}N and ^1H - ^{13}C base RDCs in nucleic acids, where TROSY-HSQC spectra also yield considerably improved spectral appearance relative to regular ^1H - ^{15}N and ^1H - ^{13}C HSQC spectra. The ability to extract RDCs from spectra that have optimized characteristics in terms of spectral resolution makes the ARTSY method particularly attractive for larger oligonucleotides, where resonance overlap associated with spectral crowding and rapid transverse relaxation invariably present a challenge. Because imino and base protons of nucleic acids resonate in reasonably well isolated regions, the effects of ^1H - ^1H dephasing during the amplitude-encoding magnetization transfer step of the TROSY experiment can be minimized by the use of band-selective pulses, obviating the need for perdeuteration, and thereby making the ARTSY amplitude encoding method applicable to the commonly used uniformly $^{13}\text{C}/^{15}\text{N}$ -enriched nucleic acids.

A second, important benefit of the use of band-selective pulses throughout the pulse sequence lies in the fact that they leave the water magnetization unperturbed. It was recently shown that band-selective BEST methods, previously developed for increasing the rate at which protein experiments can be repeated for enhanced signal-to-noise per unit of measuring time (Schanda et al. 2006; Lescop et al. 2007), are also applicable to enhancing sensitivity of imino ^1H - ^{15}N correlation experiments in nucleic acids (Farjon et al. 2009). Similarly, we here show that a comparable enhancement can be obtained for ^1H - ^{13}C correlation experiments involving the nucleic acid base protons. An added benefit of recording the ^1H - ^{13}C correlation experiments in H_2O rather than D_2O relates to the nearly 20% lower viscosity (Cho et al. 1999), which results in longer transverse relaxation times and improved spectral resolution, a detail particularly relevant for the application to larger systems.

Measurement of one-bond ^1H - ^{15}N and ^1H - ^{13}C RDCs in nucleic acids to date has been carried out almost exclusively in the frequency domain, by measurement of ^{15}N - $\{^1\text{H}\}$ (imino), ^{13}C - $\{^1\text{H}\}$ (sugar) or ^1H - $\{^{13}\text{C}\}$ (base)

doublet splittings, which represent the sum of the one-bond J coupling and the corresponding RDC. Filtering of the downfield and upfield doublet components into separate spectra, either via the inphase-antiphase (IPAP) (Ottinger et al. 1998) or individual multiplet component (IMC) selection methods (Andersson et al. 1998; Tolbert et al. 2010), largely eliminates the increased crowding associated with the doubling of the number of resonances when recording non-decoupled ^1H - ^{15}N or ^1H - ^{13}C correlation spectra. However, for both ^{15}N and aromatic base ^{13}C , the upfield doublet component has a strongly enhanced transverse relaxation rate (anti-TROSY effect). The anti-TROSY effect can be mitigated by measuring the position of a resonance which evolves as anti-TROSY magnetization for only a fraction of its evolution time (Yang et al. 1999; Kontaxis et al. 2000; Bhattacharya et al. 2010; Mantylahti et al. 2010), but this also proportionately scales down the size of the measured RDC. For ^1H - ^{13}C correlation spectra, where the IMC method separates the two ^1H - $\{^{13}\text{C}\}$ doublet components, line widths of the two components are comparable because the TROSY effect in the ^1H dimension for aromatic systems tends to be very small (Pervushin et al. 1998a). However, measurement of the relative displacement for each pair of peaks is hampered by the presence of substantial broadening in the ^1H dimension from unresolved ^1H - ^1H RDCs and difficulties in getting uniformly phased ^1H spectra when the ^1H - ^{13}C RDCs are substantial, such that selection of optimal delays in the TROSY pulse scheme cannot be achieved for all nucleotides simultaneously. Even small phase errors, which can be difficult to recognize visually in crowded spectra, can result in substantial shifts of the apparent peak position, and thereby of the corresponding RDC (Kontaxis et al. 2000).

We demonstrate the measurement of ^1H - ^{15}N and ^1H - ^{13}C RDCs from ARTSY spectra for a uniformly $^{13}\text{C}/^{15}\text{N}$ -enriched 71-nt riboswitch, RiboA, previously used as a test system for development of methods that determine the structure of such molecules from SAXS and imino ^1H - ^{15}N RDC data (Wang et al. 2009). The RDCs are fully consistent with the packed pair of stem 2 and 3 helices seen in the X-ray structure and with a static idealized A-form geometry for mutated stem 1, which differs by ca 6° relative to the X-ray structure of the native riboswitch.

Experimental Section

RiboA used in the present study contains three A-form helices, and differs from the molecule used for determining its X-ray structure (Serganov and Patel 2007) by alterations in four base pairs of helix 1, introduced to increase the stability of the molecule: G14-U82 \rightarrow G14-C82,

C15–G81 → G15–C81, U16–A80 → A16–U80, and U17–A79 → A17–U79.

Spectra presented here were recorded on three samples: an isotropic sample containing 0.7 mM RiboA in 95% H₂O/5% D₂O and a sample containing 0.8 mM RiboA in the same solvent but also including 10 mg/mL Pf1, yielding a solvent ²H quadrupole splitting of 10.1 Hz, as well as a 0.8-mM RiboA sample in the presence of 7 mg/mL Pf1 in D₂O, with a solvent ²H quadrupole splitting of 6.9 Hz. All samples additionally contained 2 mM MgCl₂, 5 mM adenine, 30 mM KCl, and 10 mM potassium phosphate buffer (pH 6.8). Sample volumes were 330 μL each, contained in Shigemi microcells.

Experimental details regarding the recording of the NMR spectra are listed in the figure legends. Unless stated otherwise, all spectra were recorded at 25°C. Spectra were processed and analyzed using NMRPipe (Delaglio et al. 1995).

Parameters used for building idealized nucleotide-specific A-form RNA were derived from a database of high resolution crystal structures, and details regarding the protocol are included as Supporting Information (SI).

Results and discussion

Measurement of imino ¹H–¹⁵N RDCs

The ARTSY pulse scheme for measurement of imino ¹H–¹⁵N RDCs is shown in Fig. 1. With the imino proton resonances mostly very well separated from the sugar and base protons, the pulse scheme is easily executed with pulses that are band-selective for the imino region. For the remainder, the experiment is very similar to the regular TROSY-HSQC experiment (Pervushin et al. 1997, 1998b), and principally differs in two aspects. First, as the J couplings and RDC values in ARTSY experiments are extracted from the transfer efficiency of magnetization from ¹H to ¹⁵N during the first INEPT step, contributions from ¹⁵N Boltzmann magnetization which normally add to the transferred magnetization must be eliminated. This is accomplished both by saturating the ¹⁵N magnetization prior to the start of the pulse scheme, and additionally by phase cycling of the ¹H 90°_{φ₁} pulse of the INEPT transfer element. Second, the duration of the first INEPT period is doubled to 1/¹J_{NH} compared to the regular TROSY-HSQC experiment, but the experiment is carried out in two modes: an attenuated mode, where the ¹H–{¹⁵N} dephasing is active during the full 1/¹J_{NH} duration, and a reference mode where the dephasing is active for only half this duration. With the exception of homonuclear RDCs to other imino protons, dephasing due to ¹H–¹H couplings during the period T is largely eliminated by the band-selective

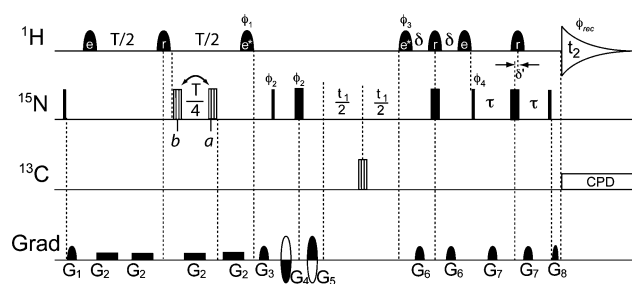


Fig. 1 ARTSY pulse sequence for measurement of imino ¹D_{NH} in nucleic acids. *Narrow and wide filled bars* represent 90° and 180° pulses, respectively, while wide *vertically hatched bars* correspond to composite 180° pulses (90_x–220_y–90_x) (Freeman et al. 1980). Composite ¹⁵N pulse marked *a* is only applied for recording the reference spectrum, pulse *b* only for the attenuated spectrum. Filled half-ellipsoids denote shaped ¹H pulses, with *e*, *e**, and *r* indicating EBURP2, time-reversed EBURP2, and ReBURP pulses, respectively (Geen and Freeman 1991). ¹H shaped pulses each have a duration of 1.0 ms (at 900.27 MHz ¹H frequency; 1.5 ms at 600 MHz) and are centered at 12.2 ppm. The ¹⁵N and ¹³C pulses are applied at 153 and 160 ppm, respectively. All pulses have phase *x* unless otherwise indicated. Delays: T = 1/J_{NH}; δ = 1.0 ms (isotropic) and 0.78 ms (Pf1) at 900 MHz (δ = 0.45 ms at 600 MHz for the isotropic sample), empirically optimized to minimize the residual ¹⁵N anti-TROSY component for the isotropic and the aligned sample, respectively; τ = 2.8 ms. Note that the last 180° ReBURP pulse is shifted toward the acquisition by δ' = 90.5 μs relative to the 180° ¹⁵N pulses such that ¹H chemical shift evolution occurring during the G₈ decoding gradient pulse (81 μs) and its recovery delay (100 μs) is refocused at the start of t₂. Phase cycling: φ₁ = *y*, –*y*; φ₂ = *y*, *y*, *x*, *x*, –*y*, –*y*, –*x*, –*x*; φ₃ = *y*, φ₄ = *y*; and φ_{rec} = *y*, –*y*, –*x*, *x*, –*y*, *y*, *x*, –*x*. Gradient pulses: G_{1,2,3,4,5,6,7,8} = 21.7, 1.19, 28.7, –39.9, 39.9, 19.6, 25.9, and 39.9 G/cm with durations of 650, 2500, 650, 400, 400, 570, 977, and 81 μs, respectively. All gradient pulses are sine bell shaped except for G₂ which is rectangular. Quadrature detection is achieved using the echo-antiecho method with the G₄ and G₅ gradient pulses as well as the φ₃ and φ₄ phases inverted and φ₂ changed to *y*, *y*, –*x*, –*x*, –*y*, –*y*, *x*, *x* for every second FID (Pervushin et al., 1998b). Fast repetition of the experiment (interscan delay of 0.6 s) can be used because H₂O magnetization remains along *z* and causes fast recovery of imino ¹H *z* magnetization. Bruker pulse sequence code included as SI

REBURP shape of the refocusing pulse (Geen and Freeman 1991), used at its mid-point. A limited degree of dephasing may remain for couplings to ¹H that are partially affected by this REBURP pulse, including protons resonating in the 8–10 ppm region, but the fractional attenuation resulting from such dephasing to a very good approximation is the same in the reference and attenuated experiment and therefore does not impact the intensity ratio, used for extracting the coupling.

Besides elimination of most ¹H–¹H RDC dephasing, a secondary benefit of using imino-selective ¹H pulses throughout the pulse scheme stems from the rapid recovery of imino magnetization through indirect magnetization transfer from the H₂O resonance. Amino NH₂ protons, in close spatial proximity to imino protons, rapidly exchange with solvent, while the use of band-selective pulses ensures that the H₂O magnetization remains close to its equilibrium

Boltzmann value. Therefore, when evaluating the intensity of the ARTSY reference spectrum as a function of the interscan delay (SI Fig. S1), a very short “apparent T_1 ” value of 0.5–0.7 s reflects the rapid magnetization transfer from water to the imino protons. Assuming zero z magnetization for the imino protons at the start of data acquisition, a delay till the start of the next scan of ca $1.3 \times T_1$ is optimal for S/N purposes, and a high repetition rate of the experiment can therefore be used (Bax et al. 1983; Farjon et al. 2009). The gain achieved by using band-selective imino proton pulses throughout, rather than non-selective pulses and a separate water suppression scheme such as WATERGATE (Piotto et al. 1992), strongly depends on the spectrometer and parameterization of the pulse sequence. Even when using non-selective pulses, at high magnetic field strengths radiation damping of the water signal will return it back to the z axis much faster than through its relatively slow longitudinal relaxation process. Therefore, depending on the instrument, the strength of gradients used, and the rate at which radiation damping takes place, a relatively short interscan delay may also be applicable for experiments that do not avoid water excitation.

As described previously (Fitzkee and Bax 2010), the magnitude of the sum of the $^1J_{\text{NH}}$ and $^1\text{H-}^{15}\text{N}$ RDC is extracted from the intensity ratio, R , observed for a given imino group in the attenuated (I_A) and reference (I_R) spectra:

$$R = I_A/I_R = \sin[\pi(^1J_{\text{NH}} + ^1D_{\text{NH}})T] / \sin[\pi(^1J_{\text{NH}} + ^1D_{\text{NH}})T/2] \quad (1)$$

which can be rewritten as:

$$^1D_{\text{NH}} = -1/T - ^1J_{\text{NH}} + (2/\pi T)\sin^{-1}(R/2). \quad (2)$$

Assuming identical noise levels, N , in the attenuated and reference spectra, the uncertainty σ in the total ($^1J_{\text{NH}} + ^1D_{\text{NH}}$) splitting extracted from the pair of spectra is given by (Fitzkee and Bax 2010):

$$\sigma = \frac{2}{\pi T(I_R/N)} \sqrt{\frac{1+R^2}{4-R^2}} \quad (3a)$$

which for the common situation where $R \ll 1$ is approximately given by

$$\sigma \approx 1/[\pi T(I_R/N)] \quad (3b)$$

As seen from Eq. 3b, the uncertainty in the derived coupling correlates inversely with the signal to noise ratio, I_R/N , in the reference spectrum and samples local minima for T durations where $R \approx 0$. The first local minimum is reached when the dephasing period, T , is $\sim 1/{}^1J_{\text{NH}}$. In principle, use of a longer T value, e.g. $2/{}^1J_{\text{NH}}$, would

reduce σ two-fold for the same I_R/N ratio. However, in practice, transverse relaxation will decrease considerably the attainable I_R/N ratio. Moreover, for larger RDC values ($|{}^1D_{\text{NH}}| \geq \sim 10$ Hz) the $R \ll 1$ approximation no longer applies for all resonances simultaneously if the $2/{}^1J_{\text{NH}}$ dephasing delay were used, thereby increasing σ (c.f. Eq. 3a), and $T \approx 1/{}^1J_{\text{NH}}$ is therefore used for all experiments.

Figure 2 compares the imino region of the reference and attenuated spectra of RiboA, aligned in Pf1. A similar set of spectra was also recorded for a sample in the absence of Pf1, where the molecule is weakly aligned due to its magnetic susceptibility anisotropy (MSA). The three helices of RiboA are packed with their axes in roughly parallel orientations (Serganov and Patel 2007; Wang et al. 2009), causing the long axis of the molecule to align parallel to the magnetic field in the Pf1 suspension, but orthogonal to the magnetic field in the isotropic sample where MSA of the nucleic acid bases dominates the alignment. As a result, in Pf1 suspension $|{}^1J_{\text{NH}} + ^1D_{\text{NH}}|$ values for the Watson–Crick base-paired imino groups are all increased relative to $|{}^1J_{\text{NH}}|$, resulting in an optimal dephasing time $T \approx 1/|{}^1J_{\text{NH}} + ^1D_{\text{NH}}| \approx 10.1$ ms.

Measurement of base $C_6\text{-H}_6$, $C_8\text{-H}_8$ and $C_2\text{-H}_2$ RDCs

Except for pyrimidine H_5 protons, carbon-attached nucleic acid base protons mostly resonate in a relatively narrow band from 6.5 to 8.5 ppm, again permitting the recording of HSQC-TROSY spectra by using band-selective ^1H pulses (Fig. 3). These experiments then are best carried out in H_2O rather than in D_2O solution, such that magnetization is rapidly transferred from water via the exchangeable amino and hydroxyl protons to the non-exchangeable protons via NOE. At 900 MHz, RiboA base proton signal intensity as observed in the first t_1 increment of the C–H ARTSY experiment of Fig. 3 for different interscan delay durations shows rapid recovery of magnetization during this delay (Fig. 4), indicative of apparent base ^1H T_1 values of ca 1.1 s. In contrast, when the experiment is carried out in D_2O , recovery of ^1H magnetization is nearly four-fold slower (SI Fig. S2). Moreover, the higher viscosity of D_2O relative to H_2O increases natural line widths by nearly 20%. The disadvantage of the use of band-selective pulses, used in the C–H ARTSY experiment of Fig. 3, is that protons resonating outside the selected bandwidth will escape detection, as applies to RiboA A21– H_2 which resonates at ~ 5.4 ppm.

Besides the usual amplitude encoding of the signal during the first INEPT transfer from $^1\text{H} \rightarrow {}^{13}\text{C}$, optimized for an average isotropic ${}^1J_{\text{CH}} = 196$ Hz by selecting $T = 5.1$ ms (the impact of different dephasing delays on the measured ${}^1J_{\text{CH}}$ value was also evaluated, see below and SI

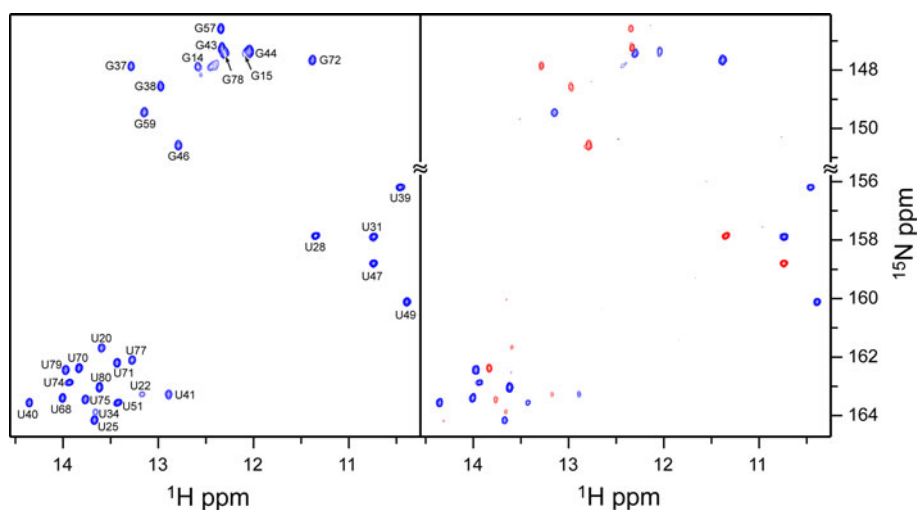


Fig. 2 Reference (*left*) and attenuated (*right*) ARTSY spectra of the imino groups in RiboA, recorded at 900 MHz ^1H frequency in the presence of 10 mg/mL Pf1. Spectra were recorded with 16 scans per FID, and the total matrix for the interleaved set of spectra comprised $2 \times 200^* \times 1024^*$ data points, with N^* referring to N complex data points, for acquisition times of 48 ms (t_1) and 84 ms (t_2). Contour levels for the attenuated spectrum are 4 times lower than shown for

the reference spectrum. The delay T (Fig. 1) was set to 10.1 ms for the Pf1-aligned sample (11.8 ms for the isotropic sample), such that in the attenuated spectrum most peak intensities are close to the null condition for RiboA. The rate at which imino proton z magnetization recovered in RiboA when the water remains along z was ca 2 s^{-1} , permitting a fast repetition of the experiment (interscan delay of 0.6 s). The total measuring time for the two interleaved spectra was ca 3 h

Table S1), the pulse scheme of Fig. 3 employs ^{13}C – ^{13}C homonuclear decoupling during the TROSY ^{13}C t_1 evolution period. This homonuclear decoupling is accomplished by a combination of a band-selective (C_2 , C_6 , C_8) REBURP-shaped pulse (Geen and Freeman 1991) followed by a broad-band composite inversion pulse, applied at the mid-point of t_1 evolution. The composite and REBURP pulses are separated by a short pulsed field gradient (G_4), needed together with G_5 for gradient-encoding of the NMR signal (Kay et al. 1992). A second composite inversion pulse is applied at the start of t_1 evolution, and serves to invert the phase error incurred by the composite pulse immediately preceding gradient G_4 (Levitt and Freeman 1981; Hwang et al. 1997). Instead of the standard non-selective 180° pulse, a ^{13}C REBURP pulse at the midpoint of the 2δ period of the TROSY transfer back to ^1H is used to eliminate ^{13}C – ^{13}C J dephasing during this period. With no significant TROSY effect achievable for base protons, composite pulse decoupling is used during data acquisition, thereby eliminating small “anti-TROSY” artifacts that result from the fact that the refocusing delay 2τ cannot be simultaneously optimized for the wide range of $^1J_{\text{CH}} + ^1D_{\text{CH}}$ values.

Figure 5 shows a small region of the reference and attenuated ARTSY spectra for the A– C_2 , A/G– C_8 and U/C– C_6 carbons in RiboA in the presence of Pf1 (See SI Fig. S3 for the isotropic spectra). Despite the substantial size of RiboA, the vast majority of ^1H – ^{13}C correlations are

sufficiently resolved for accurate quantitative intensity measurement. ^{13}C TROSY line-narrowing for the nucleic acid base carbons is slightly less effective at 900 MHz ^1H frequency than at 600 MHz (Boisbouvier et al. 1999; Ying et al. 2006), and spectra of nearly equivalent ^{13}C resolution (but decreased ^1H resolution) can be obtained at lower field strengths too (SI Fig. S4).

Measurement of pyrimidine C_5 – H_5 RDCs

Pyrimidine H_5 protons resonate in the 5–6 ppm region, very close to the water resonance. Consequently, the use of pulses that band-selectively excite these protons but leave water magnetization unaffected is not feasible. Instead, we explored two alternate solutions to record ARTSY data for obtaining the C_5 – H_5 RDCs. The first solution (Fig. 6) uses non-selective pulses, with the exception of the band-selective $^1\text{H}_5$ pulse at the mid-point of the initial INEPT transfer of magnetization from ^1H to ^{13}C , which constitutes the amplitude encoding for the ARTSY experiment. While resulting in nearly full inversion of the H_2O and H_1' resonances too, J_{HH} and D_{HH} modulation due to coupling between H_5 and $\text{H}_6/\text{H}_2/\text{H}_8$ protons is effectively eliminated by the band-selective nature of the H_5 pulse. An S^3E element (Meissner et al. 1997) is used to selectively convert the downfield TROSY $^{13}\text{C}_5$ component to z magnetization, followed by a short delay, Δ_{rd} , which serves for return of H_2O magnetization to the z axis by means of radiation

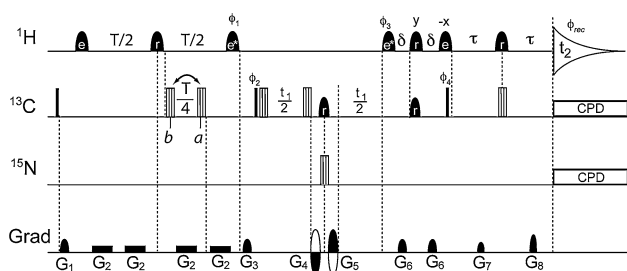


Fig. 3 ARTSY pulse sequence optimized for simultaneous measurement of base $^{13}\text{C}_{\text{C2-H2}}$, $^{13}\text{C}_{\text{C6-H6}}$ and $^{13}\text{C}_{\text{C8-H8}}$ in H_2O . Narrow and wide filled bars represent 90° and 180° pulses, respectively, while wide vertically hatched bars correspond to composite 180° pulses ($90_x-220_y-90_x$) (Freeman et al. 1980). Composite ^{13}C pulse marked a is only applied for recording the reference spectrum, pulse b only for the attenuated spectrum. Filled half-ellipsoids denote shaped ^1H pulses, with e, e*, and r indicating their profiles of EBURP2, time-reverse EBURP2, and ReBURP, respectively. All the ^1H shaped pulses are $\text{H}_2/\text{H}_6/\text{H}_8$ selective and have a duration of 1.35 ms (at 900 MHz), centered at 8.1 and 8.6 ppm for the EBURP2 (and its time-reversed pulse) and ReBURP pulses, respectively. All ^{13}C pulses are centered at 145.9 ppm. The C_6 selective ReBURP pulses have a duration of 700 μs (at 226.37 MHz ^{13}C frequency; 50% longer at 150.9 MHz) and are applied to refocus the chemical shift evolution of C_2/C_8 of purines and C_6 of pyrimidines and to remove the $^1J_{\text{C6C5}}$ coupling. The ^{15}N carrier is set to 190 ppm. All pulses have phase x unless otherwise indicated. Delays $T = 1/{}^1J_{\text{CH}}$ (see also footnote to SI Table S1); $\delta = 295 \mu\text{s}$ (empirically optimized for minimizing the anti-TROSY ^{13}C component; note that $^1J_{\text{CH}}$ evolution also occurs for ca 60% of the total durations of the time-reversed EBURP2 and the EBURP2 pulses; the ^1H and ^{13}C REBURP pulses in the middle of 2δ delays are left-aligned to reduce the $^1J_{\text{CH}}$ evolution during these two pulses; accordingly, the timing for application of the $90^\circ_{\phi_4}$ ^{13}C pulse is adjusted such that the ^{13}C chemical shift evolution is refocused during this spin-state-selective coherence transfer); $\tau = 485 \mu\text{s}$ (additional $^1J_{\text{CH}}$ evolution for $\sim 80\%$ of the ^1H ReBURP pulse duration also occurs). Phase cycling: $\phi_1 = y, -y$; $\phi_2 = x, x, -x, -x$; $\phi_3 = y$; $\phi_4 = 4(y), 4(-y)$; and $\phi_{\text{rec}} = x, -x, -x, x, -x, x, x, -x$. Gradient pulses: $G_{1,2,3,4,5,6,7,8} = 14.7, 1.19, 37.1, -35, 35, 4.9, 7, \text{ and } 42 \text{ G/cm}$ with durations of 1000, 1100, 1000, 500, 500, 79, 251, and 251 μs , respectively. All gradient pulses have a sine bell profile, except for G_2 which is rectangular. Quadrature detection is achieved using the echo-antiecho method, inverting the G_4 and G_5 gradient pulses as well as ϕ_3 for every second FID (Kay et al. 1992). Bruker pulse sequence code available as SI

damping. A subsequent $^{13}\text{C}_5$ evolution period, employing the same combination of a pair of composite inversion pulses, combined with a band-selective $^{13}\text{C}_5$ REBURP pulse as was used for $\text{C}_2/\text{C}_6/\text{C}_8$ detection (Fig. 3), is followed by a non-selective gradient-enhanced “Rance-Kay” readout scheme (Palmer et al. 1991; Kay et al. 1992). In order to suppress the strong water signal, it is essential to use relatively strong pulsed field gradients, and only on room temperature probeheads equipped with three-axis pulsed field gradients can we suppress the water signal to levels comparable to the thermal noise (Fig. 7a, b). As pointed out above, the strong advantage of recording nucleic acid spectra in the presence of fully relaxed H_2O magnetization lies in the rapid recovery of nucleic acid

z magnetization, through hydrogen exchange of the $\text{C}_2'/$ hydroxyl and base NH_2 protons, and subsequent NOE to non-exchangeable protons. This allows again for short delays between scans (Fig. 8a), thereby improving signal-to-noise, in addition to the narrower line width obtained in H_2O compared to the more viscous D_2O alternative. Note that, due to the reliance of the experiment on radiation damping, the water magnetization will attenuate strongly when the repetition rate is too fast, decreasing the z magnetization of the nucleic acid protons (Fig. 8a). Moreover, in particular U– H_5 tends to have few or no nearby exchangeable protons and recovery of its magnetization by transfer from H_2O typically will involve multiple NOE steps.

An alternate ARTSY way to measure C_5 – H_5 RDCs (Fig. 9) encodes the size of the coupling again in the transfer of magnetization from H_5 to C_5 , followed by selection of the downfield ^{13}C – $\{^1\text{H}\}$ doublet component by means of an S^3E element, and a mixed-time ^{13}C evolution period (Ying et al. 2007a). However, instead of transferring this C_5 magnetization to its directly attached H_5 , the antiphase $^{13}\text{C}_5$ – $\{^{13}\text{C}_6\}$ magnetization is converted to antiphase $^{13}\text{C}_6$ – $\{^{13}\text{C}_5\}$ magnetization, followed by a $(2J_{\text{C}_5\text{C}_6})^{-1}$ rephasing delay and a reverse INEPT transfer of $^{13}\text{C}_6$ magnetization back to $^1\text{H}_6$ for detection. Use of H_6 band-selective pulses during this last transfer step, combined with pulsed field gradients, permits effective suppression of the H_2O signal. The final spectrum (Fig. 7c, d) correlates H_6 protons with C_5 carbons. The experiment again allows for short interscan delays (Fig. 8b), with water radiation damping taking place during the mixed-time $^{13}\text{C}_5$ evolution period (of minimum duration 2Δ) and additionally the subsequent $^{13}\text{C}_6$ rephasing delay, 2Δ (Fig. 9).

The experiment is also readily modified into a 3D experiment by converting the $(2J_{\text{C}_5\text{C}_6})^{-1}$ rephasing delay into a constant-time or mixed-time $^{13}\text{C}_6$ evolution period. However, this extension was found to be unnecessary for RiboA, in part due to the excellent resolution in the $^{13}\text{C}_5$ dimension afforded by the superior TROSY property of this nucleus. This $\text{C}_5(\text{C}_6)\text{H}_6$ -ARTSY experiment detects H_6 protons that resonate relatively far away from the H_2O resonance, and water suppression therefore presents little problem and can be accomplished with single-axis z -gradients, as commonly available on cryogenic probeheads. However, the increased signal-to-noise ratio attainable by the use of such a probehead over the use of a room-temperature probehead in our experiments was more than offset by the increased magnetization transfer losses when comparing this experiment to the C_5H_5 -ARTSY experiment (Fig. 6). RDC values for C_5H_5 measured with the different pulse schemes and different ARTSY dephasing time T are presented in SI Table S2.

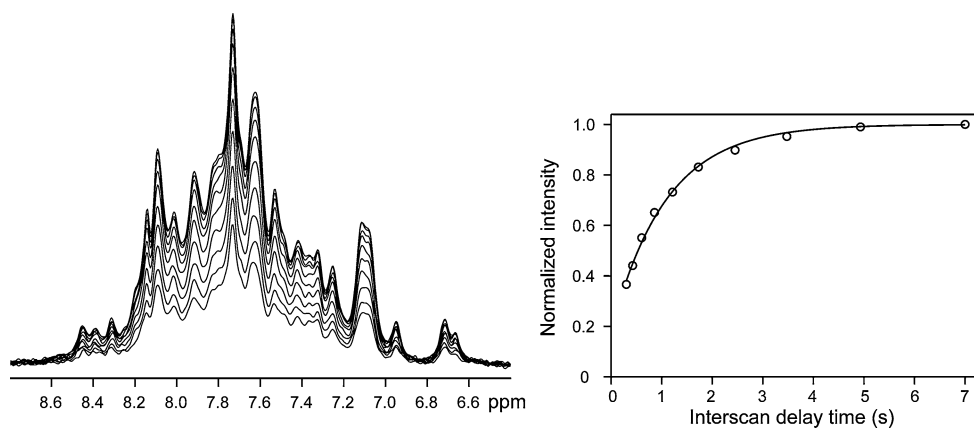


Fig. 4 Recovery of H_2 , H_6 and H_8 magnetization as a function of interscan delay in the C–H ARTSY experiment of Fig. 3. The 1D spectra shown (left) correspond to the first FID of the 900 MHz ARTSY reference experiment, and have been recorded for interscan

delays ranging from 0.3 to 7 s. Recovery of the overlapping 1H resonances is not fully exponential, indicating a range of recovery rates but can be fitted with $I(t) = I_{eq}[1 - 0.82\exp(-t/1.08s)]$ (right panel)

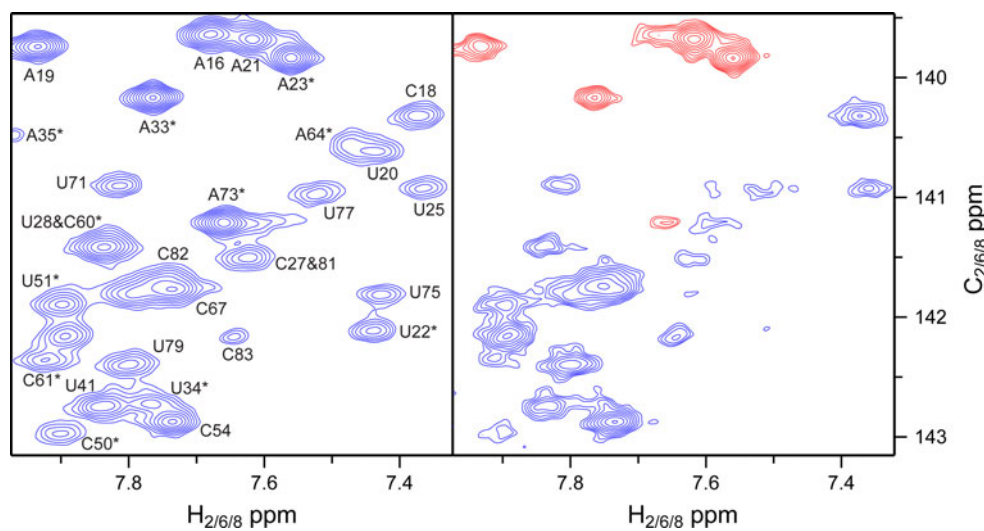


Fig. 5 Small region of the reference (left) and attenuated (right) ARTSY spectra of the $^{13}C_{6,8}$ - 1H moieties in RiboA, recorded at 900 MHz 1H frequency in the presence of 10 mg/mL Pf1. Spectra were recorded with 24 scans per FID, and the total matrix for the interleaved set of spectra comprised $2 \times 256^* \times 1,024^*$ data points, with N^* referring to N complex data points, for acquisition times of 49 ms (t_1) and 63 ms (t_2). Contour levels for the attenuated spectrum are at a level 5 times lower than shown for the reference spectrum.

The delay T (Fig. 3) was set to 4.5 ms. Due to the substantial differences in isotropic $^1J_{CH}$ couplings ($U/C \ ^1J_{C6H6} \approx 180 \pm 1$ Hz; $A/G \ ^1J_{C8H8} \approx 215 \pm 1$ Hz; $A \ ^1J_{C2H2} \approx 200 \pm 1$ Hz, all values in the absence of MSA alignment) a close-to-null condition cannot be established for all types of carbons simultaneously and $A/G \ C_8$ - H_8 are all negative (red contours). Assignments marked with asterisks correspond to nucleotides outside the helical stem regions. The total measuring time for the two interleaved spectra was ca 5.3 h

Accuracy of $^1D_{NH}$ RDCs derived from ARTSY spectra

Evaluation of the accuracy of RDCs derived from any given measurement method depends on availability of a “gold standard”, and a good fit of observed RDCs to an experimental structure does not guarantee the absence of systematic errors. For example, if all RDCs measured by any given method were underestimated by 10% this would not impact the fit to an atomic model but simply reduce the fitted alignment tensor by 10%. For proteins we have previously shown that ARTSY-derived RDCs are in excellent

agreement with ^{15}N frequency-based measurements using the IPAP-HSQC experiment (Fitzkee and Bax 2010). With a root-mean-square difference (rmsd) of 0.49 Hz, we similarly find excellent agreement between ARTSY- and IPAP-HSQC derived $^1D_{NH}$ RDCs (Fig. 10a; $R_P = 0.997$) for RiboA. This pairwise rmsd is only slightly above the average uncertainty of 0.30 Hz, derived from Eq. 3.

As is often seen for proteins, a fit of the $^1D_{NH}$ RDCs to the atomic coordinates is limited not only by the precision at which the RDCs can be measured, but also by the accuracy of the structural model, and by the assumption

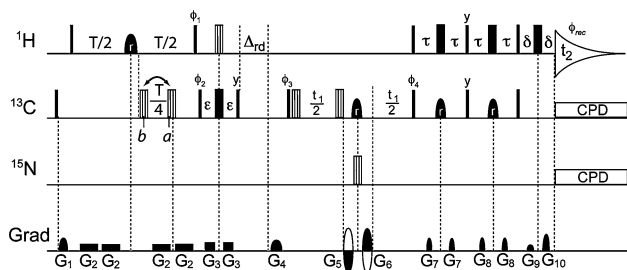


Fig. 6 C5H5 ARTSY pulse sequence optimized for measurement of pyrimidine $^1D_{C5-H5}$ in H₂O. Narrow and wide filled bars represent 90° and 180° pulses, respectively, while wide vertically hatched bars correspond to composite 180° pulses (90_x–220_y–90_x) (Freeman et al. 1980). Composite ¹³C pulse marked *a* is only applied for recording the reference spectrum, pulse *b* only for the attenuated spectrum. Filled half-ellipsoids denote shaped pulses, all of the ReBURP type. The H₅ ReBURP pulse is 1.6 ms (at 747 MHz ¹H frequency) and is centered at 4.1 ppm, while all other ¹H pulses are applied on resonance with water at 4.77 ppm. The C₅ ReBURP pulse has a duration of 800 μs (at 188 MHz ¹³C frequency). All the ¹³C pulses are centered at 101.5 ppm, except for the two composite 180° pulses immediately before and after the first $t_1/2$ period, which are applied at 130.2 ppm to invert all the C₄, C₅, and C₆ resonances for optimal $^1J_{CC}$ decoupling during t_1 . The ¹⁵N carrier is set to 155 ppm. All pulses have phase x unless otherwise indicated. Delays used in the experiments: $T = 5.7$ and 5.1 ms for the isotropic and Pf1-aligned samples, respectively; $\epsilon = 600$ μs; $\Delta_{rd} = 10$ – 15 ms, empirically optimized to let H₂O magnetization fully return to the $+z$ axis through radiation damping; $\tau = 1.2$ ms; $\delta = 353$ μs. Phase cycling: $\phi_1 = y, -y$; $\phi_2 = 4(45^\circ), 4(225^\circ)$; $\phi_3 = x, x, -x, -x$; $\phi_4 = x$; $\phi_{rec} = x, -x, -x, x, -x, x, x, -x$. Gradient pulses: G_{1,2,3,4,5,6,7,8,9,10} in the $x/y/z$ directions with strengths 7.8/7.8/0, 0/0/2.1, 0/0/9.1, 18.6/24.6/14.7, 45/45/52.5, $-45/-45/-52.5$, 0/0/6.3, 0/0/4.9, $-3/-3/-3.5$, and 42/42/49 G/cm and durations of 1700, 1216, 503, 1700, 500, 500, 779, 631, 251, 251 μs, respectively. The G_{1,4,7,8} gradient pulses are *sine bell shaped*, while the G_{2,3} gradients are rectangular and G_{5,6,9,10} are smoothed rectangular. Quadrature detection is achieved using the echo-antiecho approach with the G₅ and G₆ gradient pulses as well as the ϕ_4 pulse inverted for every other FID (Kay et al. 1992). Bruker pulse sequence code included as SI

that all RDCs are equally scaled by internal motion. RiboA contains three A-form helical stems, separated by regions of irregular structure, and with the helices 1 and 2 arranged in a roughly parallel manner, and helix 3 packed against helix 2 in an antiparallel arrangement (Serganov and Patel 2007; Wang et al. 2009). The orientations of the three helices, all roughly parallel to the z axis of the Pf1 molecular alignment tensor, result in a relatively narrow range of the ARTSY-derived $^1D_{NH}$ RDCs for the helical residues (-12 ± 5 Hz). For the RiboA sequence used in our study, four basepair switches in helix 1 were used in order to improve the stability of the aptamer relative to the sequence used for the X-ray structure (see Experimental Section), and the modeled orientation and atomic structure of helix 1 therefore contain additional uncertainty relative to those of helices 2 and 3.

$^1D_{NH}$ RDCs fit well to the coordinates of the nucleotides that are conserved relative to the prior X-ray study

(nucleotides 18–78; below referred to as “the core” of RiboA). For the 28 observable imino groups of this core (SI Table S3), an excellent fit of the RDCs to the X-ray structure is observed (Fig. 10b; rmsd = 1.65 Hz; $Q = 0.107$; $N = 28$). Very similar quality fits are obtained when using $^1D_{NH}$ RDCs obtained from an IPAP-HSQC spectrum (rmsd = 1.55 Hz; $Q = 0.100$; $N = 28$, data not shown). $^1D_{NH}$ RDCs for helix 1 also fit fairly well to a model of RiboA based on the novel G2G method (Wang et al. 2009), previously derived on the basis of SAXS data and $^1D_{NH}$ RDCs, which includes the mutated helix 1 (rmsd = 3.7 Hz; $Q = 0.22$; $N = 32$).

Interestingly, when using an empirical equation for obtaining the isotropic $^1J_{NH}$ value from the $^1H^N$ chemical shift (Ying et al. 2007b), rather than $^1J_{NH}$ splittings measured in the absence of Pf1, good agreement with the core of the RiboA structure is obtained too (Fig. 10c; rmsd = 1.60 Hz; $Q = 0.131$; $N = 28$). However, in this case the fitted alignment tensor magnitude is 22% smaller because the isotropic $^1J_{NH}$ values calculated from $^1H^N$ chemical shifts do not include the alignment resulting from magnetic susceptibility anisotropy. The $^1J_{NH}$ splittings measured in the absence of Pf1 include small RDCs which are oppositely signed compared to those induced by Pf1 alignment, thereby increasing the difference between $^1J_{NH}$ splittings measured in Pf1-free and Pf1-containing samples.

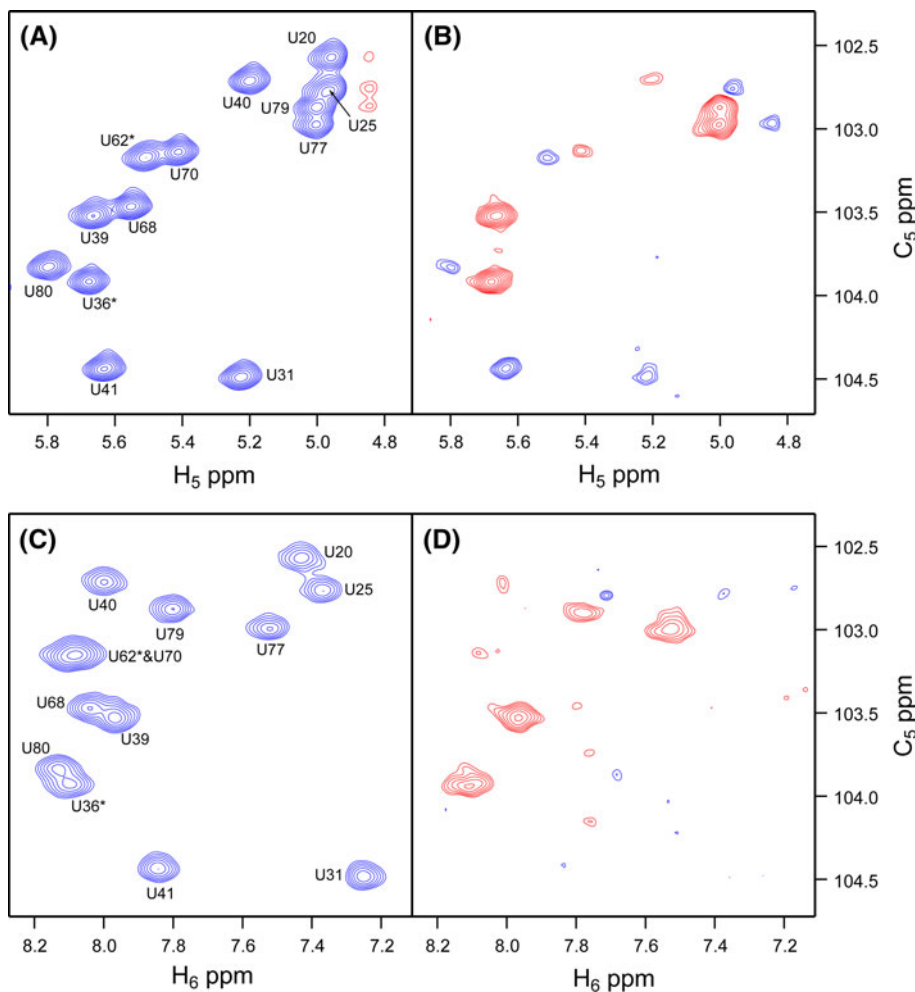
Accuracy of $^1D_{CH}$ RDCs derived for C₂, C₆ and C₈

When comparing $^1D_{CH}$ values derived with the ARTSY and IMC methods, excellent agreement is seen for the $A^{-1}D_{C2H2}$ values, but substantial systematic differences are seen for $^1D_{C6H6}$ and $^1D_{C8H8}$ values, where IMC-derived RDCs are smaller by ca 4 and 2 Hz, respectively (Fig. 11a). Fits of the $^1D_{CH}$ RDCs to the RiboA structure require assignment of the corresponding ¹H and ¹³C spectra, a non-trivial task for a molecule the size of RiboA. Assignments used in this study are based on a novel Global Structure Aided Bayesian method (Wang et al. unpublished results), supplemented by 3D NOESY and through-bond J-connectivity data.

Figure 11b shows the correlation between the experimental ARTSY-derived $^1D_{CH}$ RDCs for the core of RiboA and values predicted for the X-ray structure on the basis of the $^1D_{NH}$ derived alignment tensor. Bond lengths used in these analyses ($r_{NH} = 1.043$ Å for G and 1.057 Å for U; $r_{CH} = 1.104$ Å) are adjusted such that they include the effect of zero-point librations and vibrations (Ying et al. 2006; Grishaev et al. 2009).

As noted previously, accurate measurement of one-bond splittings in the ¹H dimension using the IMC method can be impacted by cross-correlated relaxation between 1H – 1H

Fig. 7 Sections of the reference (*left*) and attenuated (*right*) ARTSY spectra of the U $^{13}\text{C}_5\text{-}^1\text{H}_5$ moieties in RiboA, recorded in the presence of 10 mg/mL Pf1. Contour levels for the attenuated spectra are drawn at levels that are 5 times lower than shown for the corresponding reference spectrum. **a, b** Spectra recorded at 747 MHz with the pulse scheme of Fig. 6, using a dephasing interval of $T = 5.1$ ms, employing a room temperature 3-axis gradient probehead, with 8 scans per FID, and an interscan delay of 1.5 s, for a total measurement time of ca 9 h for the interleaved $2 \times 600^* \times 512^*$ data matrix (with $t_{1,\text{max}} = 72$ ms, $t_{2,\text{max}} = 43$ ms). **c, d** Spectra recorded at 600 MHz with the C5(C6)H6-ARTSY pulse scheme of Fig. 9, using a dephasing interval of $T = 5.2$ ms, employing a cryogenic probehead equipped with a z gradient, using 128 scans per FID, and an interscan delay of 0.7 s, for a total measurement time of ca 32 h for the interleaved $2 \times 150^* \times 512^*$ data matrix (with $t_{1,\text{max}} = 75$ ms, $t_{2,\text{max}} = 47$ ms)



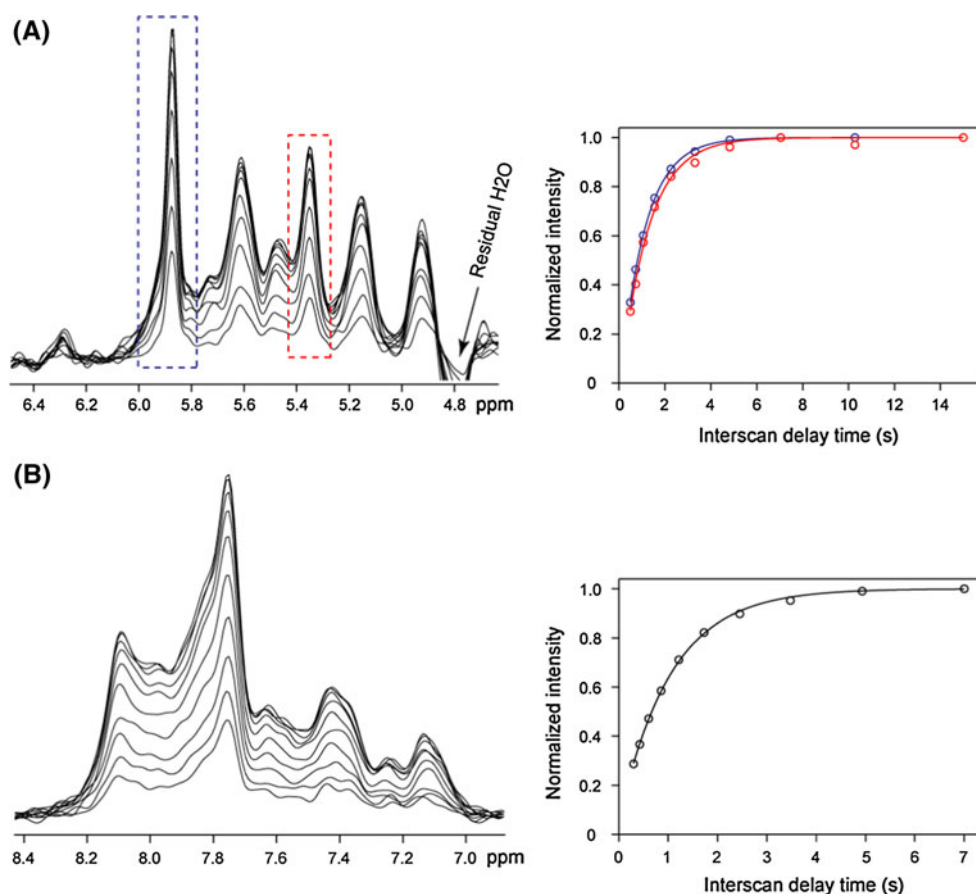
and $^1\text{H}\text{-}^{13}\text{C}/^{15}\text{N}$ dipolar interactions, which gives rise to asymmetry in the unresolved $^1\text{H}\text{-}^1\text{H}$ multiplet (Tjandra and Bax 1997b; de Alba and Tjandra 2006a, b; Grishaev et al. 2008). Notably, for A-H₂ and A/G-H₈ protons in the isotropic sample, which lack $^1\text{H}\text{-}^1\text{H}$ splittings, ARTSY- and IMC- derived $^1\text{J}_{\text{CH}}$ splittings agree closely (pairwise rmsd 1.7 Hz). In contrast, in the aligned sample unresolved RDC between H₈ and H_{2'_{i-1}} combined with cross-correlated relaxation by the $^{13}\text{C}_8\text{-}^1\text{H}_8$ and $^1\text{H}_8\text{-}^1\text{H}_{2'_{i-1}$ dipolar mechanisms results in a systematic underestimate of the actual splitting (-1.7 ± 3.2 Hz) when measured in the ^1H dimension. The magnitude of this effect scales with the size of the $^1\text{H}\text{-}^1\text{H}$ RDC which is proportional to the geometric factor, $3\cos^2\theta - 1$, where θ is the angle between the $^1\text{H}\text{-}^1\text{H}$ vector and the C-H bond, which varies substantially, even within A-form helical regions (SI Table S4).

The IMC-derived RDC values also show considerably worse agreement with values predicted on the basis of the X-ray structure for the core of RiboA (rmsd = 6.7 Hz; $Q = 0.21$; $N = 36$) than $^1\text{D}_{\text{NH}}$ values, and tend to underestimate the actual RDC values. Comparison of observed and

predicted ARTSY-derived $^1\text{D}_{\text{CH}}$ RDCs also show increased scatter compared to what was observed for $^1\text{D}_{\text{NH}}$ (Fig. 11b; rmsd = 3.5 Hz; $Q = 0.11$; $N = 36$), but to a much lesser degree. In part this could be caused by errors in the alignment tensor which was derived from a limited number of 28 $^1\text{D}_{\text{NH}}$ couplings. Indeed, a better fit is obtained when using an SVD fit between experimental $^1\text{D}_{\text{CH}}$ RDCs of the core of RiboA and coordinates of the X-ray structure (rmsd = 2.8 Hz; $Q = 0.086$; $N = 36$; Fig. 11c). Importantly, there is no systematic under- or over-estimate of the ARTSY $^1\text{D}_{\text{CH}}$ couplings relative to values predicted on the basis of the $^1\text{D}_{\text{NH}}$ - derived alignment tensor, confirming validity of the effective r_{NH} and r_{CH} bond lengths used in our analysis.

Considering the substantial range of isotropic $^1\text{J}_{\text{CH}}$ values, from 180 Hz for $^1\text{J}_{\text{C}_6\text{H}_6}$ to 215 Hz for $^1\text{J}_{\text{C}_8\text{H}_8}$, no single T duration satisfies the requirement to yield a close-to-zero intensity for the resonances of all base $^{13}\text{C}\text{-}^1\text{H}$ groups in the attenuated ARTSY spectrum. However, as can be seen from Eq. 3, the requirement for a close-to-zero intensity is not particularly stringent. Indeed, repeating the CH-ARTSY measurement on the Pf1 containing sample for

Fig. 8 Recovery of H_5 magnetization as a function of interscan delay in **a** the C_5-H_5 ARTSY experiment of Fig. 6 (747 MHz), recorded in H_2O , and **b** the $C_5(C_6)H_6$ ARTSY experiment of Fig. 9 (600 MHz). The 1D spectra (left) correspond to the first FID of the ARTSY reference experiment, and have been recorded for interscan delays ranging from 0.5 to 15 s in **a** and from 0.3 to 7 s in **b**. Recovery of the overlapping 1H resonances is not fully exponential, indicating a range of recovery rates, which is adequately fitted with **a** $I(t) = I_{eq}[1 - 1.07\exp(-t/1.21s)]$ (red boxed 1H resonance) or $I(t) = I_{eq}[1 - 1.07\exp(-t/1.07s)]$ (blue boxed resonance), and **(B)** $I(t) = I_{eq}[1 - 0.95\exp(-t/1.05s)]$



four different T durations yielded $^1J_{CH} + ^1D_{CH}$ values that (with few exceptions, e.g. A17 C_8H_8 and U20 and U25 C_6H_6) do not vary by more than the S/N-derived uncertainties (SI Table S1).

Accuracy of $^1D_{C_5H_5}$ RDCs

Comparison of the RDCs measured at 750 MHz 1H frequency on a room temperature probehead with the scheme of Fig. 6 and with the ARTSY- $C_5(C_6)H_6$ experiment of Fig. 9 at 600 MHz shows a fair correlation ($R_P = 0.87$; pairwise rmsd = 7.2 Hz; $N = 33$), but is dominated by the lower signal to noise ratio of the ARTSY- $C_5(C_6)H_6$ experiment (Fig. 12a).

For the values that differ the most between the two methods, we note the following: The discrepancies between couplings measured for U51, U80 and U71 appear to be caused by partial overlap in the $C_5(C_6)H_6$ spectrum, whereas correlations for C26 and C82 were weak and therefore resulted in intrinsically large uncertainties in the corresponding RDCs. No clear reason for the discrepancy between the $^1D_{C_5H_5}$ values measured by C_5H_5 and $C_5(C_6)H_6$ methods for U25 and U47 could be identified, but the fact that couplings measured by the C_5H_5 scheme fit better to the structure suggests that they are more

accurate. Except for the two outliers U25 and U71 in Fig. 12b, RDCs measured by C_5H_5 and $C_5(C_6)H_6$ methods fit about equally well to the X-ray structure of helical residues in the RiboA core (nucleotides 18–78). Our finding that the simpler C_5H_5 pulse scheme appears less prone to generate aberrant RDCs makes this the method of choice for $^1D_{C_5H_5}$ measurement, but it requires three-axis pulsed field gradient hardware if this measurement is to be carried out on an H_2O sample.

Refinement of RiboA model

The natural sequence of stem 1 in RiboA consists of $G_{13}GCUUCAUA_{21}$ base paired with $C_{83}UGAAGUAU_{75}$, but is mutated to $G_{13}GGAACAUA_{21}/C_{83}CCUUGUAU_{75}$ in the modified riboswitch used in the current study. In the X-ray structure, none of the modified base pairs make intramolecular tertiary interactions and a logical way to model stem 1 therefore is to simply model its first 5 basepairs as an ideal A-form helical extension of the top of the A-form helix 1, seen to contact the linker between helices 2 and 3 in the X-ray structure (Serganov and Patel 2007). Generation of an idealized A-form helical extension was carried out in two ways: In a first method, loose harmonic restraints for all phosphodiester backbone torsion

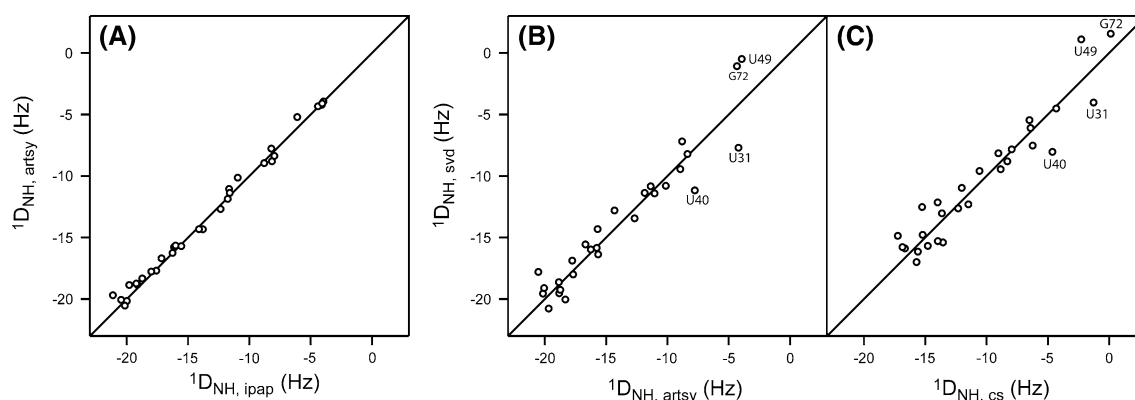


Fig. 10 Evaluation of the quality of ARTSY-derived $^1D_{NH}$ couplings for RiboA, measured at 900 MHz. **a** comparison of RDCs derived from the ARTSY spectra of Fig. 2 with those measured from an IPAP-HSQC spectrum (Yao et al. 2009). **b** Singular value decomposition (SVD) fit (Losonczi et al. 1999) of ARTSY-derived $^1D_{NH}$ couplings (SI Table S3) to the core (nucleotides 18–78) of the RiboA X-ray structure (PDB entry 1Y26), where $^1D_{NH}$ couplings are derived

from the difference in $^1J_{NH} + ^1D_{NH}$ measured in the presence and absence of 10 mg/mL Pf1. **c** Same as **b**, but using isotropic couplings calculated from the empirical equation that predicts $^1J_{NH}$ from the 1H chemical shift (i.e., lacking an MSA-induced $^1D_{NH}$ contribution) (Ying et al. 2007a). Uncertainties of the experimentally derived RDCs in all panels are comparable and smaller than the size of the *open circles* for the majority of residues (see SI Table S3)

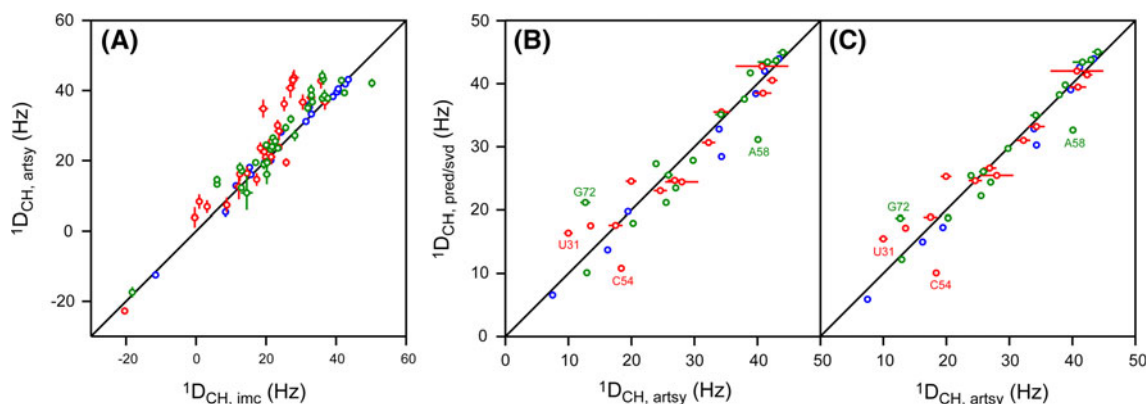


Fig. 11 Evaluation of the quality of ARTSY-derived $^1D_{CH_{2H_2}}$ (blue), $^1D_{C_6H_6}$ (red) and $^1D_{C_8H_8}$ (green) values measured for RiboA. Outliers are labeled. **a** Comparison of ARTSY- and IMC-derived $^1D_{CH}$ values. The values from the ARTSY experiment with $T = 4.9$ ms at 900 MHz (Table S1) are used in the *plot*. Nucleotide specific assignments are not yet available for a subset of the values shown, including the three $^{13}C-^1H$ pairs with negative RDCs. **b** Comparison of ARTSY-derived RDCs (average of all the 5 sets given in Table S1) with $^1D_{CH}$ values predicted for the core (nucleotides 18–78) of the X-ray structure

(PDB entry 1Y26), using the $^1D_{NH}$ derived alignment tensor (rmsd = 3.5 Hz; $Q = 0.11$; $N = 36$). **c** SVD fit of the same $^1D_{CH}$ values as in **b** to the X-ray coordinates of the core of RiboA (rmsd = 2.8 Hz; $Q = 0.086$; $N = 36$). The highly reproducible, negative RDCs seen in **a** correspond to nucleotides yielding intense, narrow cross peaks, indicative of large amplitude internal dynamics, and are not compatible with any base C–H vector in the X-ray structure

RDC values obtained for helices 2 and 3 of RiboA fit well to the X-ray structure of this oligonucleotide, and the facile measurement of a large set of base RDCs offers valuable constraints in determining a high quality solution structure of this riboswitch once resonance assignments are completed.

In the absence of resonance overlap, the size limit of systems to which the ARTSY method is applicable is governed by the attainable signal-to-noise ratio in the reference spectrum (cf eq 3b). Considering that the shape of RiboA is highly prolate, its rotational diffusion is quite

anisotropic. However, under the conditions studied (at 25°C), transverse ^{15}N relaxation rates and $^{15}N\{-^1H\}$ dipolar/CSA transverse cross-correlation rates (both measured in the presence of Pf1) correspond to rates expected for isotropic rotational diffusion with correlation times of 17.4 ± 3.7 ns, where the large range reflects the different orientations of the imino groups relative to the long axis of the molecule. Upon lowering the temperature to 10°C, transverse ^{15}N and cross-correlated relaxation rates (measured on the same sample) increase by ca 70%, corresponding to an effective correlation time of ca 30 ns. At

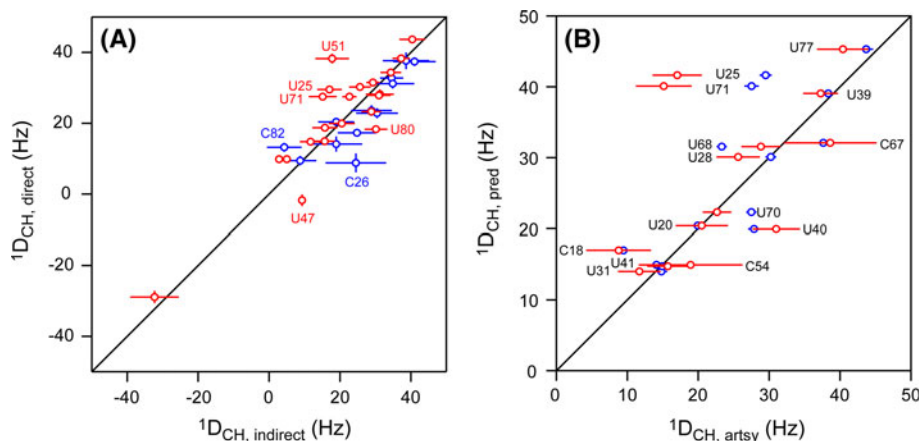


Fig. 12 Evaluation of $^1D_{C5H5}$ values measured for RiboA by direct (C5H5) and indirect (C5(C6)H6) ARTSY methods. **a** Plot of directly measured $^1D_{C5H5}$ values extracted from the 747-MHz ARTSY spectra of Fig. 7a and b with values derived from the indirect 600 MHz C5(C6)H6 ARTSY spectra of Fig. 7c and d. U and C nucleotides are in red and blue, respectively. **b** Correlation between predicted $^1D_{C5H5}$ values using SVD fit parameters obtained by fitting all $^1D_{CH}$ and

$^1D_{NH}$ of the core residues (SI Tables S1 and S3), versus the directly (C5H5, blue, 750 MHz) or indirectly (red, C5(C6)H6, 600 MHz) derived $^1D_{C5H5}$ RDCs. In both panels, the averaged values of two indirectly H_6 -detected C_5 - H_5 RDCs at 600 MHz are used, while for the directly detected RDCs only one set of values on the H_2O sample was collected (SI Table S2)

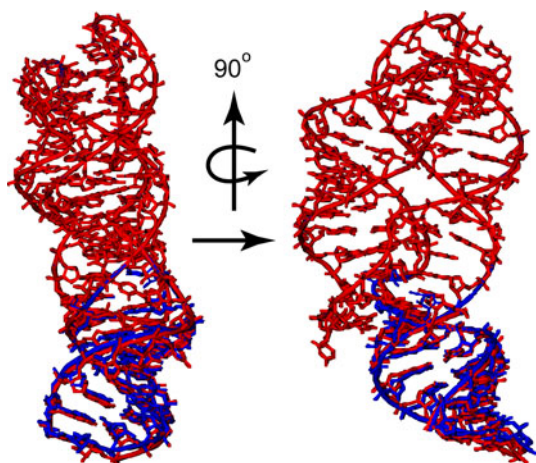


Fig. 13 Superposition of the X-ray structure of RiboA with the mutated, idealized A-form helix 1 extending the original top half of this helix (blue) and a model where helix 1 is reoriented by 6° (red) to yield optimal agreement to helix 1 RDCs

this lower temperature, the signal to noise ratio in the reference ARTSY spectrum drops by ca 65% for the base ^{13}C correlations (C_2 , C_6 and C_8), and by ca 50% for the imino correlations. For base ^{13}C - 1H pairs, 30 ns therefore approaches the intrinsic correlation time limit where useful RDCs can be measured in a reasonable amount of time. Accurate RDC measurement for the C_5 carbons is somewhat more difficult than for C_2 , C_6 and C_8 , and it appears that 20–25 ns is the upper limit for correlation times where these RDCs remain measurable by the methods presented here. The imino ^{15}N - 1H RDC measurements are less affected by the lower temperature than the aromatic ^{13}C - 1H pairs, owing to the favorable TROSY 1H and ^{15}N

line widths, and these RDCs can be measured even for systems tumbling somewhat slower than 30 ns.

Acknowledgments This work was supported by the Intramural Research Programs of the NIDDK and NCI, NIH, and by the Intramural AIDS-Targeted Antiviral Program of the Office of the Director, NIH.

References

- Andersson P, Annala A, Otting G (1998) An alpha/beta-HSQC-alpha/beta experiment for spin-state selective editing of IS cross peaks. *J Magn Reson* 133:364–367
- Bax A, Grishaev A (2005) Weak alignment NMR: a hawk-eyed view of biomolecular structure. *Curr Opin Struct Biol* 15:563–570
- Bax A, Griffey RH, Hawkins BL (1983) Correlation of proton and nitrogen-15 chemical shifts by multiple quantum NMR. *J Magn Reson* 55:301–315
- Bhattacharya A, Revington M, Zuiderweg ERP (2010) Measurement and interpretation of N-15-H-1 residual dipolar couplings in larger proteins. *J Magn Reson* 203:11–28
- Boisbouvier J, Brutscher B, Simorre JP, Marion D (1999) C-13 spin relaxation measurements in RNA: Sensitivity and resolution improvement using spin-state selective correlation experiments. *J Biomol NMR* 14:241–252
- Boisbouvier J, Delaglio F, Bax A (2003) Direct observation of dipolar couplings between distant protons in weakly aligned nucleic acids. *Proc Natl Acad Sci USA* 100:11333–11338
- Bouvignies G, Bernado P, Meier S, Cho K, Grzesiek S, Bruschweiler R, Blackledge M (2005) Identification of slow correlated motions in proteins using residual dipolar and hydrogen-bond scalar couplings. *Proc Natl Acad Sci USA* 102:13885–13890
- Cho CH, Urquidi J, Singh S, Robinson GW (1999) Thermal offset viscosities of liquid H_2O , D_2O , and T_2O . *J Phys Chem B* 103:1991–1994
- Clore GM (2000) Accurate and rapid docking of protein-protein complexes on the basis of intermolecular nuclear Overhauser

- enhancement data and dipolar couplings by rigid body minimization. *Proc Natl Acad Sci USA* 97:9021–9025
- de Alba E, Tjandra N (2006a) Interference between cross-correlated relaxation and the measurement of scalar and dipolar couplings by quantitative J. *J Biomol NMR* 35:1–16
- de Alba E, Tjandra N (2006b) On the accurate measurement of amide one-bond N-15-H-1 couplings in proteins: Effects of cross-correlated relaxation, selective pulses and dynamic frequency shifts. *J Magn Reson* 183:160–165
- Delaglio F, Grzesiek S, Vuister GW, Zhu G, Pfeifer J, Bax A (1995) NMRpipe—a multidimensional spectral processing system based on Unix pipes. *J Biomol NMR* 6:277–293
- Evenas J, Mittermaier A, Yang DW, Kay LE (2001) Measurement of C-13(alpha)-C-13(beta) dipolar couplings in N-15, C-13, H-2-labeled proteins: Application to domain orientation in maltose binding protein. *J Am Chem Soc* 123:2858–2864
- Farjon J, Boisbouvier J, Schanda P, Pardi A, Simorre JP, Brutscher B (2009) Longitudinal-Relaxation-Enhanced NMR Experiments for the Study of Nucleic Acids in Solution. *J Am Chem Soc* 131:8571–8577
- Fitzkee NC, Bax A (2010) Facile measurement of H-1-N-15 residual dipolar couplings in larger perdeuterated proteins. *J Biomol NMR* 48:65–70
- Freeman R, Kempell SP, Levitt MH (1980) Radiofrequency pulse sequences which compensate their own imperfections. *J Magn Reson* 38:453–479
- Geen H, Freeman R (1991) Band-selective radiofrequency pulses. *J Magn Reson* 93:93–141
- Grishaev A, Ying J, Canny MD, Pardi A, Bax A (2008) Solution structure of tRNA(Val) from refinement of homology model against residual dipolar coupling and SAXS data. *J Biomol NMR* 42:99–109
- Grishaev A, Yao LS, Ying JF, Pardi A, Bax A (2009) Chemical Shift Anisotropy of Imino N-15 Nuclei in Watson-Crick Base Pairs from Magic Angle Spinning Liquid Crystal NMR and Nuclear Spin Relaxation. *J Am Chem Soc* 131:9490–9492
- Hansen DF, Vallurupalli P, Kay LE (2008a) Quantifying two-bond (HN)-H-1-(CO)-C-13 and one-bond H-1(alpha)-C-13(alpha) dipolar couplings of invisible protein states by spin-state selective relaxation dispersion NMR spectroscopy. *J Am Chem Soc* 130:8397–8405
- Hansen DF, Vallurupalli P, Kay LE (2008b) Using relaxation dispersion NMR spectroscopy to determine structures of excited, invisible protein states. *J Biomol NMR* 41:113–120
- Hwang TL, van Zijl PCM, Garwood M (1997) Broadband adiabatic refocusing without phase distortion. *J Magn Reson* 124:250–254
- Kay LE, Keifer P, Saarinen T (1992) Pure absorption gradient enhanced heteronuclear single quantum correlation spectroscopy with improved sensitivity. *J Am Chem Soc* 114:10663–10665
- Kontaxis G, Clore GM, Bax A (2000) Evaluation of cross-correlation effects and measurement of one-bond couplings in proteins with short transverse relaxation times. *J Magn Reson* 143:184–196
- Kuszewski J, Schwieters C, Clore GM (2001) Improving the accuracy of NMR structures of DNA by means of a database potential of mean force describing base-base positional interactions. *J Am Chem Soc* 123:3903–3918
- Lescop E, Schanda P, Brutscher B (2007) A set of BEST triple-resonance experiments for time-optimized protein resonance assignment. *J Magn Reson* 187:163–169
- Levitt MH, Freeman R (1981) Compensation for pulse imperfections in NMR spin-echo experiments. *J Magn Reson* 43:65–80
- Losonczi JA, Andrec M, Fischer MWF, Prestegard JH (1999) Order matrix analysis of residual dipolar couplings using singular value decomposition. *J Magn Reson* 138:334–342
- Mantylahti S, Koskela O, Jiang P, Permi P (2010) MQ-HNCO-TROSY for the measurement of scalar and residual dipolar couplings in larger proteins: application to a 557-residue IgFLNa16–21. *J Biomol NMR* 47:183–194
- Meissner A, Duss JO, Sorensen OW (1997) Spin-state-selective excitation. Application for E.COSY-type measurement of J(HH) coupling constants. *J Magn Reson* 128:92–97
- Ottiger M, Delaglio F, Bax A (1998) Measurement of J and dipolar couplings from simplified two-dimensional NMR spectra. *J Magn Reson* 131:373–378
- Palmer AG, Cavanagh J, Wright PE, Rance M (1991) Sensitivity improvement in proton-detected 2-dimensional heteronuclear correlation NMR-spectroscopy. *J Magn Reson* 93:151–170
- Permi P, Rosevear PR, Annala A (2000) A set of HNCO-based experiments for measurement of residual dipolar couplings in N-15, C-13, (H-2)-labeled proteins. *J Biomol NMR* 17:43–54
- Pervushin K, Riek R, Wider G, Wuthrich K (1997) Attenuated T-2 relaxation by mutual cancellation of dipole-dipole coupling and chemical shift anisotropy indicates an avenue to NMR structures of very large biological macromolecules in solution. *Proc Natl Acad Sci USA* 94:12366–12371
- Pervushin K, Riek R, Wider G, Wuthrich K (1998a) Transverse relaxation-optimized spectroscopy (TROSY) for NMR studies of aromatic spin systems in C-13-labeled proteins. *J Am Chem Soc* 120:6394–6400
- Pervushin KV, Wider G, Wuthrich K (1998b) Single transition-to-single transition polarization transfer (ST2-PT) in [N15, H1]-TROSY. *J Biomol NMR* 12:345–348
- Peti W, Meiler J, Bruschweiler R, Griesinger C (2002) Model-free analysis of protein backbone motion from residual dipolar couplings. *J Am Chem Soc* 124:5822–5833
- Piotto M, Saudek V, Sklenar V (1992) Gradient-tailored excitation for single-quantum NMR spectroscopy of aqueous solutions. *J Biomol NMR* 2:661–665
- Prestegard JH, Al-Hashimi HM, Tolman JR (2000) NMR structures of biomolecules using field oriented media and residual dipolar couplings. *Q Rev Biophys* 33:371–424
- Schanda P, Van Melckebeke H, Brutscher B (2006) Speeding up three-dimensional protein NMR experiments to a few minutes. *J Am Chem Soc* 128:9042–9043
- Serganov A, Patel DJ (2007) Ribozymes, riboswitches and beyond: regulation of gene expression without proteins. *Nat Rev Genet* 8:776–790
- Skrynnikov NR, Kay LE (2000) Assessment of molecular structure using frame-independent orientational restraints derived from residual dipolar couplings. *J Biomol NMR* 18:239–252
- Skrynnikov NR, Goto NK, Yang DW, Choy WY, Tolman JR, Mueller GA, Kay LE (2000) Orienting domains in proteins using dipolar couplings measured by liquid-state NMR: Differences in solution and crystal forms of maltodextrin binding protein loaded with beta-cyclodextrin. *J Mol Biol* 295:1265–1273
- Tjandra N, Bax A (1997a) Direct measurement of distances and angles in biomolecules by NMR in a dilute liquid crystalline medium. *Science* 278:1111–1114
- Tjandra N, Bax A (1997b) Measurement of dipolar contributions to (1)J(CH) splittings from magnetic-field dependence of J modulation in two-dimensional NMR spectra. *J Magn Reson* 124:512–515
- Tolbert BS, Miyazaki Y, Barton S, Kinde B, Starck P, Singh R, Bax A, Case DA, Summers MF (2010) Major groove width variations in RNA structures determined by NMR and impact of C-13 residual chemical shift anisotropy and H-1-C-13 residual dipolar coupling on refinement. *J Biomol NMR* 47:205–219
- Tolman JR (2002) A novel approach to the retrieval of structural and dynamic information from residual dipolar couplings using several oriented media in biomolecular NMR spectroscopy. *J Am Chem Soc* 124:12020–12030
- Tolman JR, Ruan K (2006) NMR residual dipolar couplings as probes of biomolecular dynamics. *Chem Rev* 106:1720–1736

- Vallurupalli P, Hansen DF, Kay LE (2008) Structures of invisible, excited protein states by relaxation dispersion NMR spectroscopy. *Proc Natl Acad Sci USA* 105:11766–11771
- van Ingen H, Korzhnev DM, Kay LE (2009) An Analysis of the Effects of H-1(N)-H-1(N) Dipolar Couplings on the Measurement of Amide Bond Vector Orientations in Invisible Protein States by Relaxation Dispersion NMR. *J Phys Chem B* 113:9968–9977
- Vijayan V, Zweckstetter M (2005) Simultaneous measurement of protein one-bond residual dipolar couplings without increased resonance overlap. *J Magn Reson* 174:245–253
- Wang JB, Zuo XB, Yu P, Xu H, Starich MR, Tiede DM, Shapiro BA, Schwieters CD, Wang YX (2009) A Method for Helical RNA Global Structure Determination in Solution Using Small-Angle X-Ray Scattering and NMR Measurements. *J Mol Biol* 393:717–734
- Yang DW, Venters RA, Mueller GA, Choy WY, Kay LE (1999) TROSY-based HNCO pulse sequences for the measurement of (HN)-H-1-N-15, N-15-(CO)-C-13, (HN)-H-1-(CO)-C-13, (CO)-C-13-C-13(alpha) and (HN)-H-1-C-13(alpha) dipolar couplings in N-15, C-13, H-2-labeled proteins. *J Biomol NMR* 14:333–343
- Yao L, Vogeli B, Torchia DA, Bax A (2008) Simultaneous NMR study of protein structure and dynamics using conservative mutagenesis. *J Phys Chem B* 112:6045–6056
- Yao LS, Ying JF, Bax A (2009) Improved accuracy of N-15-H-1 scalar and residual dipolar couplings from gradient-enhanced IPAP-HSQC experiments on protonated proteins. *J Biomol NMR* 43:161–170
- Ying JF, Grishaev AE, Bax A (2006) Carbon-13 chemical shift anisotropy in DNA bases from field dependence of solution NMR relaxation rates. *Magn Reson Chem* 44:302–310
- Ying JF, Chill JH, Louis JM, Bax A (2007a) Mixed-time parallel evolution in multiple quantum NMR experiments: sensitivity and resolution enhancement in heteronuclear NMR. *J Biomol NMR* 37:195–204
- Ying JF, Grishaev A, Latham MP, Pardi A, Bax A (2007b) Magnetic field induced residual dipolar couplings of imino groups in nucleic acids from measurements at a single magnetic field. *J Biomol NMR* 39:91–96
- Zhang Q, Sun XY, Watt ED, Al-Hashimi HM (2006) Resolving the motional modes that code for RNA adaptation. *Science* 311:653–656
- Zhang Q, Stelzer AC, Fisher CK, Al-Hashimi HM (2007) Visualizing spatially correlated dynamics that directs RNA conformational transitions. *Nature* 450:1263–1267